# Diversity of structural behavior in vertebrate conventional myosins complexed with actin

**Hiroyuki Iwamoto**[1,*], **Kazuhiro Oiwa**[2], **Mihály Kovács**[3,4], **James R. Sellers**[3], **Takuya Suzuk**[1,†], **Jun'ichi Wakayama**[1,5,‡], **Takumi Tamura**[5,§], **Naoto Yagi**[1], and **Tetsuro Fujisawa**[5]

*1Research & Utilization Division, SPring-8, Japan Synchrotron Radiation Research Institute, Hyogo 679-6198 JAPAN*

*2Kansai Advanced Research Center, National Institute of Information & Communications Technology, Kobe 651-2492, JAPAN*

*3Laboratory of Molecular Physiology, National Heart, Lung and Blood Institute, National Institutes of Health, Bethesda, Maryland 20892-1762, USA.*

*4Department of Biochemistry, Eötvös University, Pázmány stny. 1/C, H-1117 Budapest, HUNGARY*

*5Labolatory of Structural Biochemistry, RIKEN Harima Institute, Hyogo 679-6148 JAPAN*

## Summary

Low-resolution three-dimensional structures of acto-myosin subfragment-1 (S1) complexes were retrieved from X-ray fiber diffraction patterns, recorded either in the presence or absence of ADP. The S1 was obtained from various myosin-II isoforms from vertebrates, including rabbit fast-skeletal and cardiac, chicken smooth and human non-muscle IIA and IIB species, and was diffused into an array of overstretched, skinned skeletal muscle fibers. The S1 attached to the exposed actin filaments according to their helical symmetry. Upon addition of ADP, the diffraction patterns from acto-S1 showed an increasing magnitude of response in the order as listed above, with features of a lateral compression of the whole diffraction pattern (indicative of increased radius of the acto-S1 complex) and an enhancement of the 5th layer-line reflection. The structure retrieval indicates that these changes are mainly due to the swing of the light chain (LC) domain in the direction consistent with the cryoelectron-microscopic results. In the non-muscle isoforms, the swing is large enough to affect the manner of quasi-crystal packing of the S1-decorated actin filaments and their lattice dimension, with a small change in the twist of actin filaments. Variations also exist in the behavior of the 50K-cleft, which apparently opens upon addition of ADP to the non-muscle isoforms but not to other isoforms. The fast-skeletal S1 remains as the only isoform that does not clearly exhibit either of the structural changes. The results indicate that the "conventional" myosin-II isoforms exhibit a wide variety of structural behavior, possibly depending on their functions and/or the history of molecular evolution.

## Keywords

myosin subfragment-1; myosin-II; ADP; X-ray fiber diffraction

*Corresponding author: Hiroyuki Iwamoto, Ph.D. Research and Utilization Div. SPring-8, Japan Synchrotron Radiation Research Institute 1-1-1 Kouto, Sayo-cho Sayo-gun, Hyogo 679-6198 JAPAN e-mail: iwamoto@spring8.or.jp
†present address: Faculty of Environmental Engineering, University of Kitakyusyu, Fukuoka, 808-0135, JAPAN
‡present address: Instrumentation Engineering Laboratory, National Food Research Institute, Ibaraki 305-8642 JAPAN
§present address: Godo Shusei Co. Ltd., Matsudo, Chiba 271-0064 JAPAN

## Introduction

Since the milestone achievement of crystal structure determination of skeletal myosin subfragment-1 (S1) in its apo (nucleotide-free) form,[1,2] a number of crystal structures have been determined for S1's from various sources and with various kinds of ligands, as summarized.[3,4] These series of studies have made it clear that (1) the whole S1 consists of the globular motor domain (which contains actin- and nucleotide-binding sites) and the largely α-helical light chain domain (which binds two or more light chains), and (2) the angle made between the two domains is highly variable, giving rise to a wide range of LC-domain orientations, depending on the source of S1 and the ligand that the S1 binds in the nucleotide pocket. In many models, the ligand-dependent change of the LC-domain orientation is considered directly responsible for force production by myosin (e.g., ref.[2]).

The variety of LC-domain orientations is not only observed in the crystal structures of S1 alone, but also in the S1 complexed with F-actin. The 3D reconstruction from cryoelectron microscopic (cryo-EM) images show that the appearances of F-actins decorated with brush-border myosin I,[5,6] chicken gizzard smooth muscle myosin II,[7] and myosin VI[8] are strikingly different from each other, and the major difference is in their LC-domain orientations.

Within the conventional myosin II isoforms alone (many of them responsible for muscle contraction), a variety of LC-domain orientations have been reported from cryo-EM studies. The LC domain of the acto-smooth muscle S1 complex shows a large change of orientation when it binds ADP[7,9,10] but in contrast, the LC domain of the acto-fast skeletal S1 stays immobile.[10,11] X-ray fiber diffraction is another sensitive method to detect structural changes, and has also shown results corresponding to the EM observations: The diffraction pattern from acto-smooth S1 complex shows a large change upon addition of ADP,[12] while the change is more subtle in the case of acto-fast skeletal S1 (for full-filament-overlap fibers see refs.[13,14] These X-ray fiber diffraction results have been discussed in the context of the LC-domain swing, but the inherent difficulty in retrieving molecular structures from diffraction patterns have prevented the diffraction studies from providing independent support or criticism to the cryo-EM results.

Here we have developed a procedure to retrieve low-resolution molecular structures of acto-S1 complexes from their diffraction patterns. This procedure is to make use of the knowledge about the known crystal structure of S1 and actin, their published docking models and the helical symmetry of F-actin. The procedure enabled us to determine, not only the most likely structures of the acto-S1 complex in the presence and absence of ADP, but also the variability or disorder that the molecules are expected to have under physiological conditions. The targets for structural retrieval were not confined to fast-skeletal and smooth muscle isoforms, but also other members of vertebrate myosin-II family, including cardiac/slow-skeletal and non-muscle IIA and IIB isoforms. These non-muscle isoforms are involved in cytokinesis and other cytoskeleton-related motility. The IIA isoform is ubiquitously distributed among various tissues and has a relatively low duty ratio (fractional time spent on actin),[15] while the IIB isoform is enriched in the central nervous system and has a high duty ratio.[16,17] The results indicate that the "ancestral" (smooth and non-muscle) isoforms show a large LC-domain swing and 50K cleft opening upon ADP binding, but fast-skeletal and cardiac isoforms show smaller or little responses. These differences in ADP sensitivities do not seem to be directly correlated with the ADP affinity of respective isoforms. Parts of the present results have been presented in an abstract form.[18]

## Results

### Diffraction patterns from acto-S1 complexes and their response to ADP

Figure 1 shows the diffraction patterns recorded from an array of overstretched skeletal muscle fibers, to which S1 from various sources had been diffused in the absence of nucleotides. As has been reported, the actin-based layer line reflections (ALL's) are strongly enhanced, because the thin filaments in the fibers are decorated with S1 following their helical symmetry.[19] Most of the intensities of the 1st to 5th, and a substantial part of the 6th and 7th ALL's come from the scattering by the attached S1 (the layer line nomenclature is based on a 13/6 helical symmetry of actin, in which 13 actin monomers exist in six turns within a short single-stranded 5.9 nm-pitch helix). The intensity profiles of major ALL's are shown in Figure 2 (dots). In each panel of Figure 2, the profiles from the ADP form (red) are superposed on those from the apo form (blue), and it is immediately noticed that the intensity profiles obtained from different S1 isoforms show a great variation in ADP sensitivity as well as in the apo profiles themselves.

Addition of 1 mM ADP causes little change in the diffraction pattern from acto-fast-skeletal S1 (Figure 1(a,b), see also ref.[20]). In the intensity profiles, ADP causes slight broadening of the 6th ALL, and slight intensification of the 2nd and 5th ALL's (Figure 2(a)). The relative insensitivity of the acto-S1 structure to ADP agrees with previous reports of ESR[11] and cryo-EM.[10]

The diffraction patterns from acto-cardiac S1 resemble those of acto-fast-skeletal S1 (Figure 1(c,d)). Although the intensity profile of the 6th ALL is similar to that of acto-fast-skeletal S1, its multi-peak nature, or lattice sampling, is evident (Figure 2(b)). This property is ascribed to the crystal packing of the acto-S1 complexes as will be described. The intensity of the outer (away from the meridian) part of the ALL increases upon ADP binding. The 5th ALL is single-peaked in both apo and ADP forms, but its peak intensity increases substantially upon ADP binding, as in the case of acto-smooth S1.

The diffraction pattern from acto-smooth S1 in the apo form (Figure 1(e)) is substantially different from that from acto-fast-skeletal S1 (see ref.[12]). The most notable differences are that the 6th ALL is positioned away from the meridian and often exhibits double peaks as a result of lattice sampling. The 5th ALL has a flattened profile and also shows a double-peaked feature. Addition of ADP causes large changes in the diffraction pattern (Figure 1(f), see also ref.[12]). The double-peaked nature of the 6th ALL is lost, the 5th ALL becomes single-peaked with greater peak intensity, and now its profile resembles that for the acto-fast-skeletal S1 complex (Figure 2(c)). Other ALL's also show some intensity changes.

The diffraction patterns from acto-non-muscle S1 show the most dramatic changes upon addition of ADP, either IIA (Figure 1(g,h)) or IIB (Figure 1(i,j)). When compared with their apo patterns (Figure 1(g,i)), the ADP patterns for these isoforms (Figure 1(h,j)) show laterally compressed appearance, indicating that the whole acto-S1 structures splay out upon addition of ADP (Reflecting this, the unit cell size of the filament lattice becomes greater. See Table 1). In both isoforms, the 5th ALL is markedly enhanced by addition of ADP (Figure 2(d,e)). The multi-peaked nature of ALL's is clearly observed in the apo pattern of IIA, and the pattern of sampling is identical to that for the smooth muscle isoform. In contrast, the multi-peaked nature is not evident in the apo pattern of IIB. On the other hand, the ADP patterns for IIA and IIB are similar to each other, and their pattern of sampling is different from that for the smooth muscle isoform. As will be described in detail, the difference in the pattern of lattice sampling is explained by slightly different helical symmetries of F-actin.

## Determination of ADP dissociation constant

In the diffraction patterns from all isoforms but fast-skeletal S1, the intensity of the 5th ALL is the most sensitive to ADP binding. By utilizing this, it is possible to determine the dissociation constant for ADP in each acto-S1 complex. This is achieved by plotting the intensity change of the most ADP-sensitive region (between $1/8$ nm$^{-1}$ and $1/15$ nm$^{-1}$) of the ALL against ADP concentration (Figure 3). Theoretically, the change in the intensity is considered to be proportional to the square of the number of S1 molecules with bound ADP (square law). On this basis, the ADP dissociation constants of acto-cardiac S1, acto-smooth S1, acto-IIA S1 and acto-IIB S1 are determined to be 2.5 μM, 11.5 μM, 3.3 μM and 0.92 μM, respectively. These values are slightly higher than published data, but the inter-species difference is consistent (summarized in ref.[15]).

## Crystal packing of acto-S1 complexes

The intensity profile of the 1st ALL shows two prominent peaks, regardless of the source of S1 or the presence/absence of ADP. These two peaks cannot be reproduced by considering a single S1-decorated F-actin filament, and it is natural to consider that the peaks appear as a result of imperfect crystal packing of F-actin filaments. The position of the peaks are most readily explained if the filaments are packed in a hexagonal lattice with a unit cell size of ~40 nm, and if the occurrence of the peaks obeys a selection rule

$$- h + k + l = 3n,$$

where $h$, $k$, and $l$ are the indices for crystal lattice planes and $n$ is an integer, with $l$ being the layer line number. The two major peaks of the 1st ALL correspond to 1,0,1 and 2,1,1 reflections, respectively. The lattice that obeys this selection rule is the rhombohedral lattice, in which neighboring two F-actin filaments are staggered by $1/3$ of their basic long-pitch repeat of ~36 nm. This is analogous to the "superlattice" arrangement of myosin filaments in frog muscle[21,22], and in the present case the unit cell size of the actin superlattice is ~40 nm whereas that of the simple actin lattice is ~23 nm (= $40/\sqrt{3}$)(The hexagonal packing of undecorated F-actin filaments has been found in smooth muscle, in which the unit cell size of the simple actin lattice is 12 nm[23]). The hexagonal packing of the F-actin filaments is not due to the influence of the hexagonal lattice of endogenous myosin filaments, because the two peaks are also observed in fibers from which endogenous myosin filaments have been extracted under high ionic strength (Figure 4).

In the pattern from acto-fast-skeletal isoform, the 1st ALL is the only layer line that obviously shows such crystallographic peaks. However, the patterns from other S1 sources often show crystallographic peaks in the 6th and other ALL's as well. In the rigor patterns from cardiac, smooth and IIA isoforms, the residuals of fitting (the difference between observed and fitted intensity profiles) by using a single-filament model indicate that the crystallographic peaks of the 6th ALL occur at the same set of $h$ and $k$ as in the 1st ALL (an example of IIA is shown in Figure 5(a)). This pattern of sampling is explained by assuming a 54/25 symmetry of actin helix, instead of 13/6.

In the ADP patterns of IIA and IIB isoforms, the peaks on the 6th ALL do not share the $h$ and $k$ indices with the 1st ALL. Instead, the peaks on the 7th ALL do (Figure 5(b)). This pattern of sampling is best explained by the 13/6 helical symmetry of F-actin. These observations suggest that, in some of myosin isoforms, the ADP-induced structural change of S1 alters the twist of F-actin, and as a result, the manner of crystal packing.

## Retrieval of low-resolution 3D structures of acto-S1 complexes

It is generally hoped that the 3D structures of acto-S1 complexes can be retrieved from their diffraction patterns, and the major obstacles in doing this are the lost phase information, the

rotary-averaged (around the Z axis) nature of diffraction patterns, imperfect crystal lattice sampling and disorder. Here we used the Lorenz model[24] as the starting structure and refined it to obtain the best-fit 3D structure for each diffraction pattern, after considering the imperfect crystal packing as described above.

The process of structure retrieval consisted of three steps of fitting, the first two in the reciprocal space and the last one in the real space. In brief, the first step was to determine the best-fit α-carbon backbone structure, which was to seek the best swing angles of the LC and upper 50K domains and other parameters (Table 3). However, the matching is usually not satisfactory by this process alone (R-factor ∼ 27% for fast-skeletal S1), because the molecules in solution environment are more likely to have more structural variations than in crystals. To improve the matching, the structure determined in the first step was further refined in the second step. This process involved random redistribution of protein mass after converting the structure to an assembly of beads (but with some constraints to reject unlikely structures: see Materials and Methods for detail). After this step the R-factor was improved to 12∼15%. The third step was again to determine the α-carbon backbone structure, which would best explain the mass distribution determined in the second step. The α-carbon backbone determined in this way is usually different from that determined in the first step. The best-fit values of parameters determined in the third step are listed in Tables 1 and 2. The density of the acto-S1 complex determined at the end of the second step, and the best-fit α-carbon backbone at the end of the third step, are overlaid in Figures 6 and 7. In Figure 2, the calculated intensity profiles at the end of the second step (curves) are shown along with the observed data (dots).

The most noticeable difference seen in the fitted structure (both in density envelopes and α-carbon backbones) is the angle of the LC domain with respect to the rest of the molecule and its change upon ADP binding. The LC domain of the fast-skeletal isoform shows only a small if any swing upon ADP binding, and its azimuthal component seems to predominate.

The LC domains of other isoforms show an upward axial swing upon ADP binding, and the direction of swing is consistent with the cryo-EM results for the smooth muscle isoform.[7] The angle of swing increases in the order of cardiac < smooth muscle < IIA ≈ IIB (Table 1). Although not apparent in the display in Figure 6, all the isoforms show more or less an azimuthal component of swing of the LC domain. The azimuthal angle of the LC domain is relatively well-defined, while in many isoforms the axial angle seems to show a wider range of variability (see the discrepancy mapping of LC domain angles; Figure 8). This is especially true for the smooth muscle isoform, which seems to be composed of a mixture of populations with different LC domain angles.

As for the upper 50K domain, all the isoforms examined show a tendency of having a more closed configuration when compared with the crystal structure of chicken skeletal S1,[1] in agreement with published observations.[9,10,25,26] An opening of the domain has been reported upon ADP binding,[9] but this behavior was not confirmed in the present study. Instead, the opening of the domain is observed in the ADP structure of the IIA and IIB isoforms (Figure 7 (d,e)). None of the rest of the isoforms show any sign of opening of the domain (Figure 7 (a-c)). The lack of evidence of cleft opening upon ADP binding to the fast-skeletal isoform is in agreement with the cryo-EM result.[10]

Other parameters to be fitted include the relative occupancies of the two light chains (essential and regulatory) and tropomyosin with respect to the S1 heavy chain. The occupancy of the essential light chain is usually close to 100%, but that of the regulatory light chain is lower, and in the case of fast-skeletal isoform, the value is ∼50%. This value is coincidentally in agreement with the value reported by Holmes et al.,[26] and in their report the S1 specimen was prepared in the same manner as in the present study (papain digestion). The low occupancy

could be due to a partial loss of regulatory light chains during preparation or increased mobility in this region, resulting in a spuriously low value. The occupancy of tropomyosin is also ~60% of the starting value, and this is consistent for all the isoforms. Because the 40% loss of tropomyosin is unlikely, this low occupancy could again be due to the mobility of tropomyosin molecules on the thin filament.

## Discussion

### Structure retrieval from X-ray diffraction data

In the present study, the structures of complexes between actin and S1 from various sources were analyzed by means of X-ray fiber diffraction technique. The results allow direct comparison of the isoform-dependent differences in the magnitude of ADP-induced structural changes of S1 complexed with actin. The ADP-induced structural changes, notably the swing of the LC domain, have been reported by using cryo-EM, which has recently experienced a major technical progress in both data acquisition and processing (e.g., ref.[26]). As a tool for analyzing the medium-to-low resolution structures of macromolecules, the fiber diffraction technique has advantages over cryo-EM. The data collection is quick, and the effect of ligand becomes immediately obvious on the computer screen. Internal control is readily obtained by repeating exposure to the same specimen under different conditions. It is also suitable for dynamic measurements (for an example of time-resolved measurement see ref.[27]). The major drawback is the difficulty in the interpretation of diffraction patterns because only the amplitude of the structure factor (Fourier transform of the diffracting object) is recorded. Therefore the establishment of modeling procedures (i.e., building of real-space structure models that best explain the diffraction data) is crucial.

Recently, various algorithms have been devised for *ab initio* restoration of real-space molecular structures from the small-angle X-ray scattering profiles from "chaotically oriented" proteins in solution (e.g., refs.[28,29]). Without knowledge about pre-existing structural information, these algorithms use arbitrarily packed assemblies of pseudo-atoms as starting models, and refine the structures by using a genetic or simulated-annealing algorithm. The refined structures show a remarkable matching with crystal structures. Even in these cases, incorporation of pre-existing structural information into starting models accelerates convergence. In this respect, the situation with acto-S1 complexes is much more favorable, because of the knowledge about the symmetry according to which the molecules are arranged, the crystal structures of constituent molecules and the parts of the molecules that are likely to move. Although based on a less-sophisticated least-squares algorithm, our fitting procedure was able to achieve reasonable convergence with R-factors of 12~15%. The retrieved structures are generally consistent with the cryo-EM structures reported earlier, in the behavior of both the LC domain and the 50K cleft.

### Relation to earlier studies

Of the five myosin-II isoforms analyzed here, two have been studied extensively in the context of structural change upon ADP binding: fast-skeletal and smooth muscle isoforms. The insensitivity of the fast-skeletal isoform to ADP is consistent with many previous results (references cited in Results) in that the LC domain shows little axial swing and the 50K cleft remains closed. However, the present results raise a possibility that the LC domain may swing azimuthally. In the discrepancy contour of LC angles (Figure 8), the azimuthal angles of LC domain in the apo- and ADP forms seem stable and are confined to narrow ranges. On the other hand, the axial angles are more widely spread in both forms. This feature is shared by other isoforms, and may indicate the greater mobility of the LC domain in the axial (a little skewed) direction.

Although the present results for the fast-skeletal isoform are consistent with many other studies using S1, a number of papers have reported larger structural changes of the fast-skeletal isoform. These include X-ray diffraction studies[13,14,30] and an electron-microscopic study.[31] These studies use muscle fibers with full filament overlap, or heavy meromyosin preparation in which the two heads of a myosin molecule are connected in the C-terminal part. As has been discussed,[30] the difference may come from the connection of the LC domain to the thick filament backbone, or at least the subfragment-2 portion that unites the two heads, as they could mechanically influence the LC-domain orientation. This explanation would be plausible in the light of differential molecular stiffness in different ligand states (see below).

As for the smooth muscle isoform, a large swing (23°) has been reported from the cryo-EM studies, resulting in a 3.5 nm movement at the C-terminal end of the S1 molecule.[7] The value obtained in the present study is 29°, and is comparable to the published data. However, the minima of discrepancy in the contour map for the ADP form (Figure 8) is widely spread in the axial direction with a number of shoulders (although not apparent in the figure). This suggests that in the ADP form, the LC domain is highly mobile, and this may account for the loss of lattice sampling in ALL's except for the 1st ALL.

In addition, it has been reported that the 50K cleft opens upon ADP binding.[9] Although our results do not confirm this, we do observe such behavior in non-muscle isoforms. In these isoforms, the LC-domain angle is much more stabilized in a swung-out configuration than in the smooth muscle isoform (Figure 8). If the closure/opening of the 50K cleft is coupled with the LC-domain swing, the more variable LC angles of the smooth muscle isoform could conceal the movement of the 50K cleft.

### Magnitude of the LC-domain swing and its significance

Besides the fast-skeletal and smooth muscle isoforms, we were able to determine the swing angles of cardiac/slow-skeletal and non-muscle IIA and IIB isoforms. The results show that the magnitude of swing increases in the order of fast-skeletal < cardiac/slow-skeletal < smooth < non-muscle IIA ≈ IIB.

Initially, the swing of the LC domain was considered in the context of an additional mechanism for force production, because the direction of swing upon release of ADP agrees with the direction of power stroke. The observation in *in vitro* motility assays that the unitary displacement of smooth muscle S1 occurs in two steps[32] seemed to support this view. However, the mechanics study did not show a drop of force of smooth muscle strips upon addition of ADP as it should if reversing the second power stroke.[33] It is also argued that the swing upon ADP release cannot be a second power stroke because the step is not coupled with a large drop in free energy as in the $P_i$ release step. Alternatively, it has been proposed that the swing is a device for assuring economic force maintenance in slow myosin isoforms.[34] It has been reported that the rate of ADP release is slow enough to limit the rate of dissociation of myosin isoforms from actin.[35] Because the role of slow isoforms is to maintain force with small energy expenditure rather than sliding, the slow isoforms should keep their bound ADP, and the swing of the LC domain serves as a mechanosensitive device to provide an energy barrier against releasing ADP. This argument predicts that the affinity of respective isoforms for ADP is intimately related to the angle of LC-domain swing. Do the present results support the prediction?

The affinities of acto-S1 complex for ADP were determined here, and the values are generally consistent with published results. According to these, the cardiac/slow-skeletal isoform has a higher affinity for ADP than the smooth muscle isoform. The cardiac/slow-skeletal isoform does swing its LC domain, but its magnitude is by no means greater than that of the smooth muscle isoform. The two non-muscle isoforms have greater ADP affinities than the smooth

muscle isoform, and the affinity of the IIB isoform is about three times greater than that of the IIA isoform. Both nonmuscle isoforms show a greater LC swing than the smooth muscle isoform, but the magnitudes of LC swing of IIA and IIB isoforms are similar (The two isoforms exhibit contrasting kinetic properties, as mentioned earlier). In addition, the *Dictyostelium* (a primitive eukaryote with a single myosin II gene[38]) myosin II is believed to have a relatively low affinity for ADP[39] and is not expected to swing its LC domain, but our unpublished X-ray diffraction data suggest that it does. In terms of homology in amino acid sequences, the smooth muscle isoform is close to the non-muscle isoforms and these three isoforms form a cluster of "ancestral" proteins while the fast-skeletal isoform is distant, and the cardiac/slow-skeletal isoform is associated with it (based on the multiple-alignment tool provided by Protein Information Resource, Georgetown University, USA). Therefore, at present it seems that the swing angle of the LC domain is more related to the "phylogeny" of myosin isoforms rather than ADP affinity.

Nevertheless, these observations are not in conflict with the published argument,[34] if the elasticity or stiffness of S1 is different in rigor and in ADP forms. The present results suggest that the mobility of the LC domain is generally different in apo and ADP forms (Figure 8), and especially the ADP form of smooth muscle S1 shows greater mobility than its apo form. This is in agreement with the mechanics observation that the stiffness of smooth muscle strips decreases upon addition of ADP.[33] If so, it is possible to create a large free energy penalty in releasing ADP during tension maintenance (i.e., high ADP affinity) without making a corresponding difference in LC swing angles. In this respect, more mechanical characterization of each isoform, including *in vitro* motility assays, would be informative in further clarifying this point.

After all, based on the thermodynamic considerations,[34] an effective way of increasing the shortening velocity would be to increase the dissociation constant for ADP above its intracellular level, and making the LC angle insensitive to ADP binding (This ensures that ADP dissociates from myosin at any strain). The fast-skeletal isoform might have evolved along this line, by directing the LC domain midway between the apo- and ADP angles for those ancestral isoforms (see Table 1 and Fig. 8; see also ref.[10]). Whether this scheme of evolution can be generalized to other fast myosins (e.g., flight muscle myosin of *Drosophila*[36] and unconventional plant myosins[37]) awaits further studies.

## Behavior of the 50K cleft

The present results did not provide evidence that ADP binding opens the 50K cleft of fast-skeletal or cardiac isoforms complexed with actin. In contrast, ADP binding seems to open at least partially the 50K cleft of non-muscle isoforms, and the same has been reported to occur in the smooth muscle isoform.[9] Again, the behavior of the 50K cleft seems to follow the "phylogeny" of myosin isoforms; the characteristic is shared by these three "ancestral" isoforms. This cleft movement is considered responsible for the nucleotide-induced myosin dissociation from actin.[26,38] In this respect, it is worth noting that these three isoforms remain relatively strongly bound to actin after binding ADP, while ADP binding to fast-skeletal S1 certainly reduces the binding constant of S1 for actin (e.g., refs.[38,40]). Possible explanations for this apparent contradiction would be that (1) the stereospecific interaction between the lower 50K domain and actin has a greater contribution to the acto-S1 affinity, and (2) acto-fast-skeletal or cardiac S1 has a stronger tendency to be destabilized by an open cleft, so that the cleft remains closed as long as S1 is strongly bound to actin.

## Conclusion

The present study has established a procedure to retrieve low-resolution structures of acto-S1 complexes from their X-ray fiber diffraction data, and the procedure has proven equally

effective for all the myosin-II species tested. The retrieval has revealed that the conventional myosin-II isoforms show wide variations in ligand-dependent structural changes. The mobility of movable parts can also be assessed. With data acquisition in seconds and the retrieval of a single structure overnight, X-ray fiber diffraction can now serve as a powerful tool for obtaining a quick structural glance of unknown myosin isoforms, and for assessing the structural basis of disease-causing mutations on known myosin isoforms.

## Materials and Methods

### Proteins

The rabbit fast-skeletal S1 was prepared from the fast skeletal muscles of Japanese White rabbit by the method based on Margossian and Lowey[41] by papain digestion of myosin, as described.[20] The S1 from the cardiac/slow-skeletal isoform was obtained from either cardiac or soleus muscle from the same strain by the method identical to that for the fast-skeletal S1. Smooth muscle myosin was prepared from chicken gizzard, freshly obtained from a local poultry slaughterhouse, by the method published previously.[42,43] The obtained myosin was papain-digested to obtain S1, and a higher concentration of papain was needed than for fast-skeletal S1. In all cases, the digestion was terminated by adding antipain (Sigma-Aldrich), and the S1 was finally purified by gel-filtration (Superdex 200 HR 10/30, Pharmacia). The non-muscle isoforms were expressed in a baculovirus expression system, as described,[15,16] and were stored in liquid nitrogen until use.

### Preparation of specimens for X-ray diffraction

The S1 prepared as describe above was diffused into an array of ~30 overstretched, skinned rabbit psoas muscle fibers in the absence of nucleotide, as described.[20,27] The concentration of S1 in the loading solution was usually 2 mg/ml or more, as this concentration is necessary for effective labeling.[44] The loading was usually done for more than 24 hr. After this, the loading solution was replaced by a rigor solution[45] which did not contain S1. The apo patterns were recorded in this solution. In addition, the solution to record ADP patterns contained up to 1 mM of ADP, 2 mM $MgCl_2$, 250 μM $AP_5A$ , 1 mg/ml glucose and 170 U/ml hexokinase (Sigma-Aldrich).

### X-ray diffraction recording

The method for X-ray diffraction recording was as described before.[20] Briefly, X-ray diffraction patterns were recorded at the BL45XU beamline (small-angle scattering station) of SPring-8,[46] by using a cooled CCD (charge-coupled device) camera (C4880, Hamamatsu Photonics, $1000 \times 1018$ pixels) in combination with an X-ray image intensifier (V5445P, Hamamatsu Photonics). The wavelength was either 0.1 or 0.09 nm, and the specimen-to-detector distance was ~2 m. To compensate for the relatively small dynamic range of the detector, absorber masks made of aluminum and copper were placed at the center of the image intensifier. The exposure time was ~2 s, and usually several to tens of patterns were summed to obtain a final image to be analyzed. The four quadrants of the image were folded after correction for the fiber inclination, and the background was subtracted as described.[47]

### Retrieval of low-resolution 3D structures

As briefly stated in Results, the process of structure retrieval consisted of three steps of fitting.

The first step was to modify the α-carbon backbone of the starting structure (Lorenz docking model for actin and chicken fast-skeletal S1,[24] downloaded from Dr. M. Lorenz's public domain server http://ergo.mpimf-heidelberg.mpg.de/~michael/. This model is based on the published coordinates of actin[48] and chicken fast-skeletal S1[1]) so that it gave the best-fit

(lowest R-factor) intensity profiles of ALL's. A segment of tropomyosin was added to the structure.[47] The fitted parameters were the swing of the LC domain and the upper 50K domain of S1, the rotation of the whole S1 molecules around its long axis, and the relative occupancies of the two light chains and the tropomyosin segment. The LC domain was made to swing around the two hinges of the "converter" domain, i.e., Gly699 and Gly710.[49] The swing angle of the segment between the two glycines was set to half of that of the LC domain. The upper 50K domain was made to swing around Gly466. The axis for rotation of the whole S1 was the line connecting Arg371 and Lys843. The angles and the occupancies were repeatedly adjusted in 1° and 1% steps, respectively, until no more improvement was obtained in the R-factor. At this stage, the fit between the observed and calculated intensity profiles was generally poor.

In the second step of fitting or refinement, the mass of the best-fit α-carbon backbone structure was redistributed into a 3D matrix (voxels; 3D analogy of pixels in 2D diagram) as an assembly of beads or "dummy atoms". The voxel size (or the minimum center-to-center distance between two beads) was $0.8 \times 0.8 \times 0.8$ nm. With this voxel size, the mass of S1 was distributed to ~710 beads. Then in an iterative procedure, the spatial distribution of the beads was altered by transferring a fraction of mass of a bead to another randomly selected bead or an empty voxel within the matrix. A transfer that yielded a better R-factor was adopted. This was repeated until the success rate decreased to a preset level. The beads representing the actin and tropomyosin molecules were left untouched. To incorporate the effect of imperfect lattice sampling, each reflection was expressed as a linear combination of a continuous function and a set of discrete sampling peaks, each of which having a finite Gaussian spread. This treatment is of empirical nature, and not based on assessment of the extent of lattice imperfectness. Both the fractions of continuous and sampled components and the unit cell size were parameters to be fitted in the second step. A total of six independent calculation runs were performed for each diffraction pattern, and the obtained structures showed a reasonable degree of consistency (see below; Table 4).

This part of fitting may be similar to other *ab initio* fitting programs that use dummy atoms. A problem inherent in this type of programs is that they tend to create a variety of structures, some of which are obviously unrealistic but equally give low R-factors. These unrealistic structures generally show excessive projections or isolated densities. To prevent such features from developing, the program used here was coded so that isolated masses were not created, and a mass transfer that increased the surface area was penalized. Even so, a projection could eventually pinch off and inadvertently create an isolated mass in the course of fitting, as seen in some of the pictures in Figures 6 and 7.

The structure obtained at the end of this process was an envelope of mass of protein that best explained the diffraction data, and the fit between the observed and calculated intensity profiles was as shown in Figure 2.

The third step was to redefine the α-carbon backbone structure of S1 that best explained the envelope determined in the second step. The LC domain angle and other parameters as determined in the first step were further adjusted so that the difference between the backbone structure and the envelope was minimized.

In the first and the second steps, the structure factor of the protein mass was calculated by performing two-dimensional fast Fourier transform, after projecting the mass of the decorated actin onto a plane. The cutoff spacing for fitting, which defined the spatial resolution, was 4 $nm^{-1}$. The software used for fittings was written in-house, and was run on Pentium 4- or Pentium D-based personal computers (Dell Co.). The CPU time needed for a single calculation in the second step (consisting of ~1,200 successful iterations) was usually one day on a Pentium-D, when two executable programs were run independently. The molecular graphics

in Figures 6 and 7 were created by using an executable version of PyMol (DeLano Scientific), and the graphics of discrepancy contour map (Figure 8) were created by using Origin (OriginLab Corp.)

## Evaluation of reproducibility in calculations

To evaluate the reproducibility of calculated results in the second step, the cross-correlated normalized spatial discrepancy (NSD)[50] was calculated for all possible combinations within the results from six independent calculation runs by using a program package DAMAVER. [51] The NSD values were calculated for the S1 part alone. NSD has been proposed as a measure of superposability of two structures, and it generally fell within the range of 0.4-0.5 in the present calculations (Table 4). An NSD value of 0.6 or less is regarded to indicate overall similarity of models.[51] None of the calculated structures fell outside the range of the mean ± 2SD (standard deviation).

## References

1. Rayment I, Rypniewski WR, Schmidt-Base B, Smith R, Tomchick DR, Benning MM, Winkelmann DA, Wesenberg G, Holden HM. Three-dimensional structure of myosin subfragment-1: A molecular motor. Science 1993;261:50–58. [PubMed: 8316857]

2. Rayment I, Holden HM, Whittaker M, Yohn CB, Lorenz M, Holmes KC, Milligan RA. Structure of the actin-myosin complex and its implications for muscle contraction. Science 1993;261:58–65. [PubMed: 8316858]

3. Sellers, JR. Myosins. Oxford University Press; Oxford, UK: 1999.

4. Holmes KC, Schroder RR, Sweeney HL, Houdusse A. The structure of the rigor complex and its implications for the power stroke. Phil. Trans. R. Soc. B 2004:1819–1828. [PubMed: 15647158]

5. Jontes JD, Wilson-Kubalek EM, Milligan RA. A 32-degree tail swing in brush border myosin I on ADP release. Nature 1995;378:751–753. [PubMed: 7501027]

6. Jontes JD, Milligan RA. Brush border myosin-I structure and ADP-dependent conformational changes revealed by cryoelectron microscopy and image analysis. J. Cell Biol 1997;139:683–693. [PubMed: 9348285]

7. Whittaker M, Wilson-Kubalek EM, Smith JE, Faust L, Milligan RA, Sweeney HL. A 35-Å movement of smooth muscle myosin on ADP release. Nature 1995;378:748–751. [PubMed: 7501026]

8. Wells AL, Lin AW, Chen L-Q, Safer D, Cain SM, Hasson T, Carragher BO, Milligan RA, Sweeney HL. Myosin VI is an actin-based motor that moves backwards. Nature 1999;401:505–508. [PubMed: 10519557]

9. Volkmann N, Hanein D, Ouyang G, Trybus KM, DeRosier DJ, Lowey S. Evidence for cleft closure in actomyosin upon ADP release. Nature Struct. Biol 2000;7:1147–1155. [PubMed: 11101898]

10. Volkmann N, Ouyang G, Trybus KM, DeRosier DJ, Lowey S, Hanein D. Myosin isoforms show unique conformations in the actin-bound state. Proc. Natl. Acad. Sci. USA 2003;100:3227–3232. [PubMed: 12612343]

11. Gollub J, Cremo CR, Cooke RS. ADP release produces a rotation of the neck region of smooth myosin but not skeletal myosin. Nature Struct. Biol 1996;3:796–802. [PubMed: 8784354]

12. Poole KJV, Lorenz M, Ellison P, Evans G, Rosenbaum G, Boesecke P, Holmes KC, Cremo CR. A low angle diffraction study of the structure of the actomyosin complex: effects of ADP binding. J. Muscle Res. Cell Motil 1997;18:264a.

13. Takemori S, Yamaguchi M, Yagi N. Effects of adenosine diphosphate on the structure of myosin cross-bridges: an X-ray diffraction study on a single skinned frog muscle fibre. J. Muscle Res. Cell Motil 1995;16:571–577. [PubMed: 8750228]

14. Takezawa Y, Kim D-S, Ogino M, Sugimoto Y, Kobayashi T, Arata T, Wakabayashi K. Backward movements of cross-bridges by application of stretch and by binding of MgADP to skeletal muscle fibers in the rigor state as studies by X-ray diffraction. Biophys. J 1999;76:1770–1783. [PubMed: 10096877]

15. Kovács M, Wang F, Hu A, Zhang Y, Sellers JR. Functional divergence of human cytoplasmic myosin II. Kinetic characterization of the non-muscle IIA isoform. J. Biol. Chem 2003;278:38132–38140. [PubMed: 12847096]

16. Wang F, Kovács M, Hu A, Limouze J, Harvey EV, Sellers JR. Kinetic mechanism of non-muscle myosin IIB. Functional adaptations for tension generation and maintenance. J. Biol. Chem 2003;278:27439–27448. [PubMed: 12704189]

17. Rosenfeld SS, Xing J, Chen L-Q, Sweeney HL. Myosin IIB is unconventionally conventional. J. Biol. Chem 2003;278:27449–27455. [PubMed: 12740390]

18. Iwamoto H, Oiwa K, Uyeda TQP, Kovács M, Sellers JR, Wakayama J, Tamura T, Fujisawa T, Yagi N. Low-resolution structures of complexes between actin and myosin-II subfragments from muscle and non-muscle sources as studied by X-ray diffraction. Biophys. J. Abstr 2006:274a.

19. Goody RS, Reedy MC, Hofmann W, Holmes KC, Reedy MK. Binding of myosin subfragment 1 to glycerinated insect flight muscle in the rigor state. Biophys. J 1985;47:151–169. [PubMed: 3978197]

20. Iwamoto H, Oiwa K, Suzuki T, Fujisawa T. X-ray diffraction evidence for the lack of stereospecific protein interactions in highly activated actomyosin complex. J. Mol. Biol 2001;305:863–874. [PubMed: 11162098]

21. Huxley HE, Brown W. The low-angle X-ray diagram of vertebrate striated muscle and its behaviour during contraction and rigor. J. Mol. Biol 1967;30:383–434. [PubMed: 5586931]

22. Luther PK, Squire JM. Three-dimensional structure of the vertebrate muscle A-band. II. The myosin filament superlattice. J. Mol. Biol 1980;141:409–439. [PubMed: 6969319]

23. Rice RV, Moses JA, McManus GM, Brady AC, Blasik LM. The organization of contractile filaments in a mammalian smooth muscle. J. Cell Biol 1970;47:183–196. [PubMed: 4327514]

24. Lorenz M, Popp D, Holmes KC. Refinement of the F-actin model against X-ray fiber diffraction data by the use of a directed mutation algorithm. J. Mol. Biol 1993;234:826–836. [PubMed: 8254675]

25. Mendelson R, Morris EP. The structure of the acti-myosin subfragment-1 complex: Results of searches using data from electron micorscopy and x-ray crystallography. Proc. Natl. Acad. Sci. USA 1997;94:8533–8538. [PubMed: 9238011]

26. Holmes KC, Angert I, Kull FJ, Jahn W, Schroder RR. Electron cryo-microscopiy shows how strong binding of myosin to actin releases nucleotide. Nature 2003;425:423–427. [PubMed: 14508495]

27. Wakayama J, Tamura T, Yagi N, Iwamoto H. Structural transients of contractile proteins upon sudden ATP liberation in skeletal muscle fibers. Biophys. J 2004;87:430–441. [PubMed: 15240477]

28. Chacón P, Morán F, Diáz JF, Pantos E, Andreu JM. Low-resolution structures of proteins in solution retrieved from X-ray scattering with a genetic algorithm. Biophys. J 1998;74:2760–2775. [PubMed: 9635731]

29. Svergun DI. Restoring low resolution structure of biological macromolecules from solution scatteringusing simulated annealing. Biophys. J 1999;76:2879–2886. [PubMed: 10354416]

30. Horiuti K, Yagi N, Takemori S, Yamaguchi M. An X-ray diffraction study on the ADP-induced conformational change in skeletal muscle myosin. J. Biochem 2003;133:207–210. [PubMed: 12761183]

31. Katayama E. Quick-freeze deep-etch electron microscopy of the actin-heavy meromyosin complex during the in vitro motility assay. J. Mol. Biol 1998;278:349–367. [PubMed: 9571057]

32. Veigel C, Molloy JE, Schmitz S, Kendrick-Jones J. Load-dependent kinetics of force production by smooth muscle myosin measured with optical tweezers. Nature Cell Biol 2003;5:980–986. [PubMed: 14578909]

33. Dantzig JA, Barsotti RJ, Manz S, Sweeney HL, Goldman YE. The ADP release step of the smooth muscle cross-bridge cycle is not directly associated with force generation. Biophys. J 1999;77:386–397. [PubMed: 10388765]

34. Cremo CR, Geeves MA. Interaction of actin and ADP with the head domain of smooth muscle myosin: Implications for strain-dependent ADP release in smooth muscle. Biochemistry 1998;37:1969–1978. [PubMed: 9485324]

35. Siemankowski RF, Wiseman MO, White HD. ADP dissociation from actomyosin subfragment 1 is sufficiently slow to limit the unloaded shortening velocity in vertebrate muscle. Proc. Natl. Acad. Sci. USA 1985;82:658–662. [PubMed: 3871943]

36. Swank DM, Vishnudas VK, Maughan DM. An exceptionally fast actomyosin reaction powers insect flight muscle. Proc. Natl. Acad. Sci. USA 2006;103:17543–17547. [PubMed: 17085600]

37. Kashiyama T, Kimura N, Mimura T, Yamamoto K. Cloning and characterization of a myosin from Characean alga, the fastest motor protein in the world. J. Biochem 2000;127:1065–1070. [PubMed: 10833276]

38. Conibear PB, Bagshaw CR, Fajer PG, Kovacs M, Malnasi-Csizmadia A. Myosin cleft movement and its coupling to actomyosin dissociation. Nature Struct. Biol 2003;10:831–835. [PubMed: 14502269]

39. Ritchie MD, Geeves MA, Woodward SKA, Manstein DJ. Kinetic characterization of a cytoplasmic myosin motor domain expressed in Dictyostelium discoideum. Proc. Natl. Acad. Sci. USA 1993;90:8619–8623. [PubMed: 8378339]

40. Geeves MA. The dynamics of actin and myosin association and the crossbridge model of muscle contraction. Biochem. J 1991;274:1–14. [PubMed: 1825780]

41. Margossian SS, Lowey S. Preparation of myosin and its subfragments from rabbit skeletal muscle. Methods Enzymol 1982;85:55–71. [PubMed: 6214692]

42. Ikebe M, Hartshorne DJ. Effects of $Ca^{2+}$ on the conformation and enzymatic activity of smooth muscle myosin. J. Biol. Chem 1985;260:13146–13153. [PubMed: 2932435]

43. Persechini A, Hartshorne DJ. Ordered phosphorylation of the two 20 000 molecular weight light chains of smooth muscle myosin. Biochemistry 1983;22:470–476. [PubMed: 6687432]

44. Tamura T, Wakayama J, Fujisawa T, Yagi N, Iwamoto H. Intensity of X-ray reflections from skeletal muscle thin filaments partially occupied with myosin heads: Effect of cooperative binding. J. Muscle Res. Cell Motility 2004;25:329–335.

45. Iwamoto H. Influence of ionic strength on the actomyosin reaction steps in contracting skeletal muscle fibers. Biophys. J 2000;78:3138–3149. [PubMed: 10827990]

46. Fujisawa T, Inoue K, Oka T, Iwamoto H, Uruga T, Kumasaka T, Inoko Y, Yagi N, Yamamoto M, Ueki T. Small-angle X-ray scattering station at the SPring-8 RIKEN beamline. J. Appl. Cryst 2000;33:797–800.

47. Iwamoto H, Oiwa K, Suzuki T, Fujisawa T. States of thin filament regulatory proteins as revealed by combined cross-linking/X-ray diffraction techniques. J. Mol. Biol 2002;317:707–720. [PubMed: 11955019]

48. Kabsch W, Mannherz HG, Suck D, Pai EF, Holmes KC. Atomic structure of the actin:DNase I complex. Nature 1990;347:37–44. [PubMed: 2395459]

49. Dominguez R, Freyzon Y, Trybus KM, Cohen C. Crystal structure of a vertebrate smooth muscle myosin motor domain and its complex with the essential light chain: visualization of the pre-power stroke state. Cell 1998;94:559–571. [PubMed: 9741621]

50. Kozin MB, Svergun DI. Automated matching of high- and low-resolution structural models. J. Appl. Cryst 2001;34:33–41.

51. Volkov VV, Svergun DI. Uniqueness of ab initio shape determination in small-angle scattering. J. Appl. Cryst 2003;36:860–864.
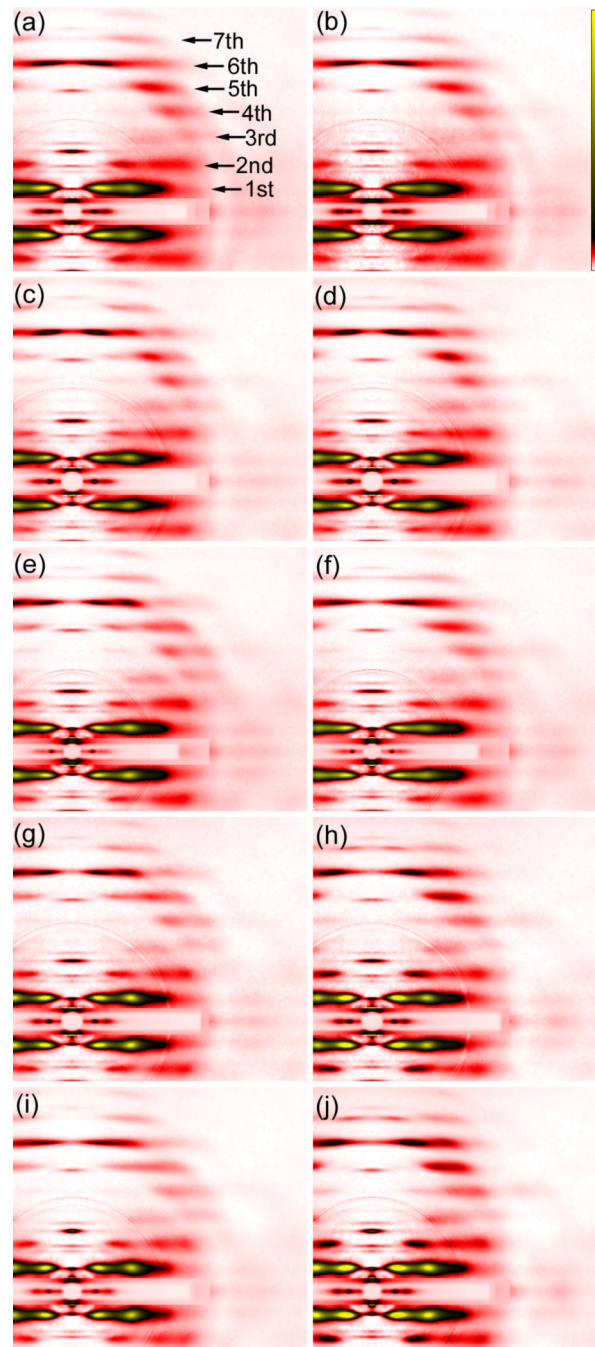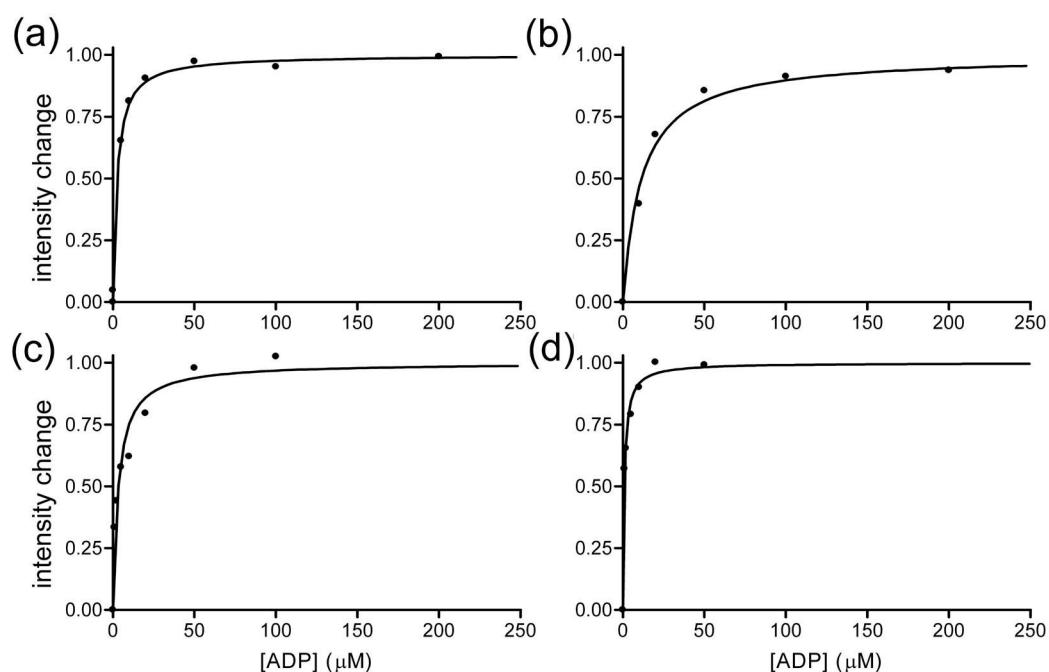
**Figure 1.**
X-ray diffraction patterns from the complex between actin and myosin S1 from various sources. (a,b) rabbit fast-skeletal; (c,d), rabbit cardiac/slow-skeletal; (e,f), chicken gizzard smooth; (g,h), human non-muscle IIA; (i,j), human non-muscle IIB. (a,c,e,g,i), apo form (in the absence of nucleotide); (b,d,f,h,j), ADP form. The apo and ADP patterns were recorded from identical specimens. The four quadrants of the patterns have been folded, and the background scattering has been subtracted. The ring-like lines around the center are due to the correction for the aluminum mask placed in front of the detector to attenuate the intense part of the pattern. The yellowish part of the 1st ALL is the area of excessively high intensity.
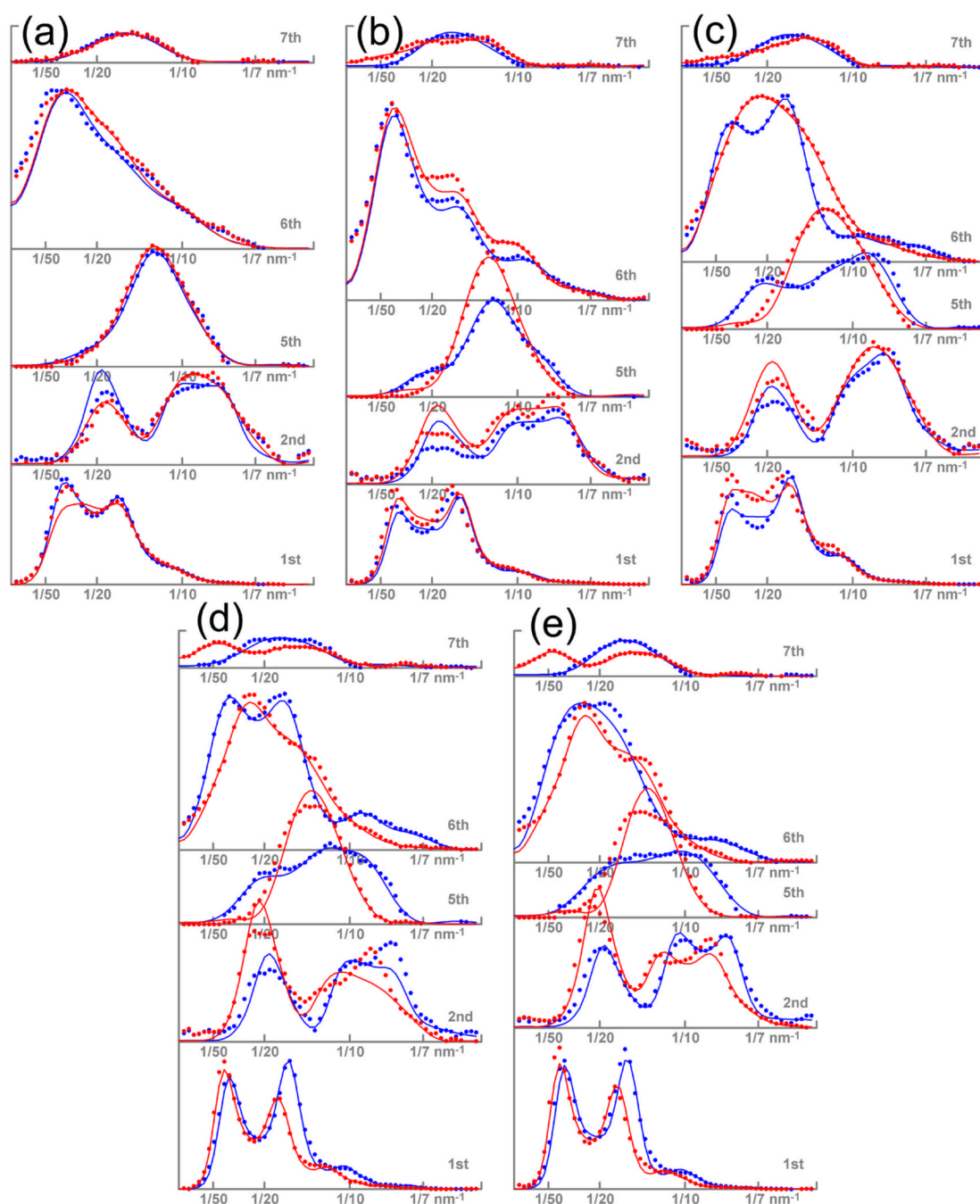
**Figure 2.**
Intensity profiles of major ALL's in the absence and presence of ADP. (a), rabbit fast-skeletal; (b), rabbit cardiac/slow-skeletal; (c), chicken gizzard smooth; (d), human non-muscle IIA; (e), human non-muscle IIB. Dots, observed intensities (Figure 1); curves, intensities calculated from the fitted structures (Figure 6). Blue, apo form; red, ADP form. The vertical scale for the 1st ALL is 1/10 of that for other ALL's.

**Figure 3.**
The dependence of the intensity of the 5th ALL on ADP concentration. (a), rabbit cardiac/slow-skeletal; (b), chicken gizzard smooth; (c), human non-muscle IIA; (d); human non-muscle IIB. The intensity is the square root of the increment above the level of apo pattern and normalized to the maximal change. The line is the best-fit one-site binding function (hyperbola) $y = x / (K_d + x)$, where $x$ is the concentration of ligand and $K_d$ is the dissociation constant.
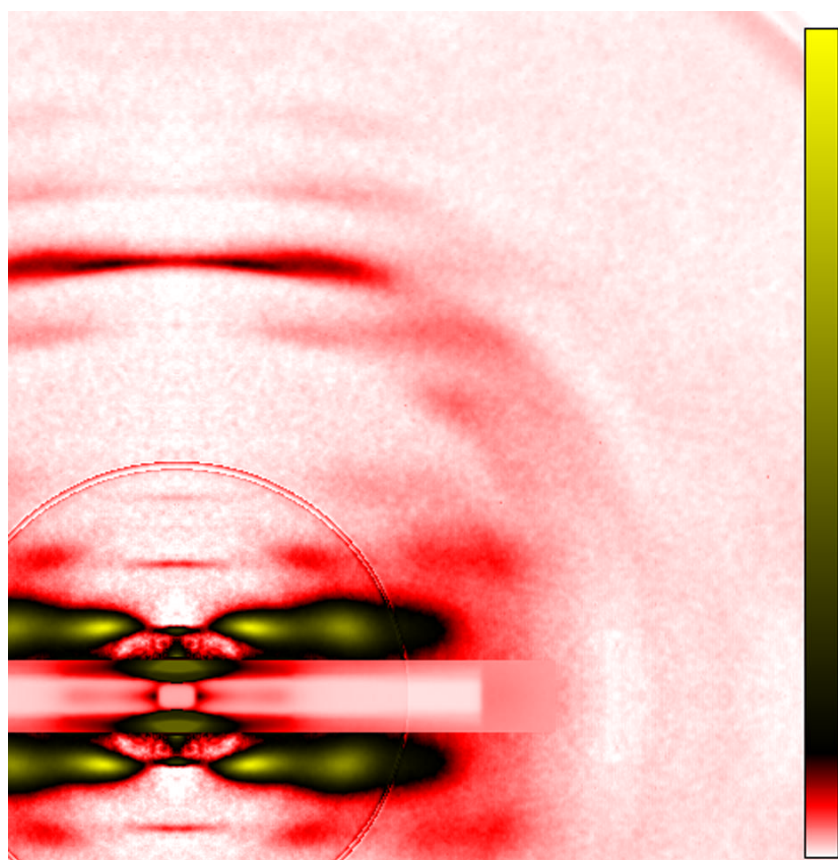
**Figure 4.**
Diffraction pattern from ghost fibers (skeletal muscle fibers pretreated with a high-ionic strength relaxing solution to extract endogenous myosin) into which chicken gizzard S1 was diffused. Note that as in the case of non-extracted fibers, the 1st ALL shows the sampled peaks originating from the hexagonal lattice of filaments.
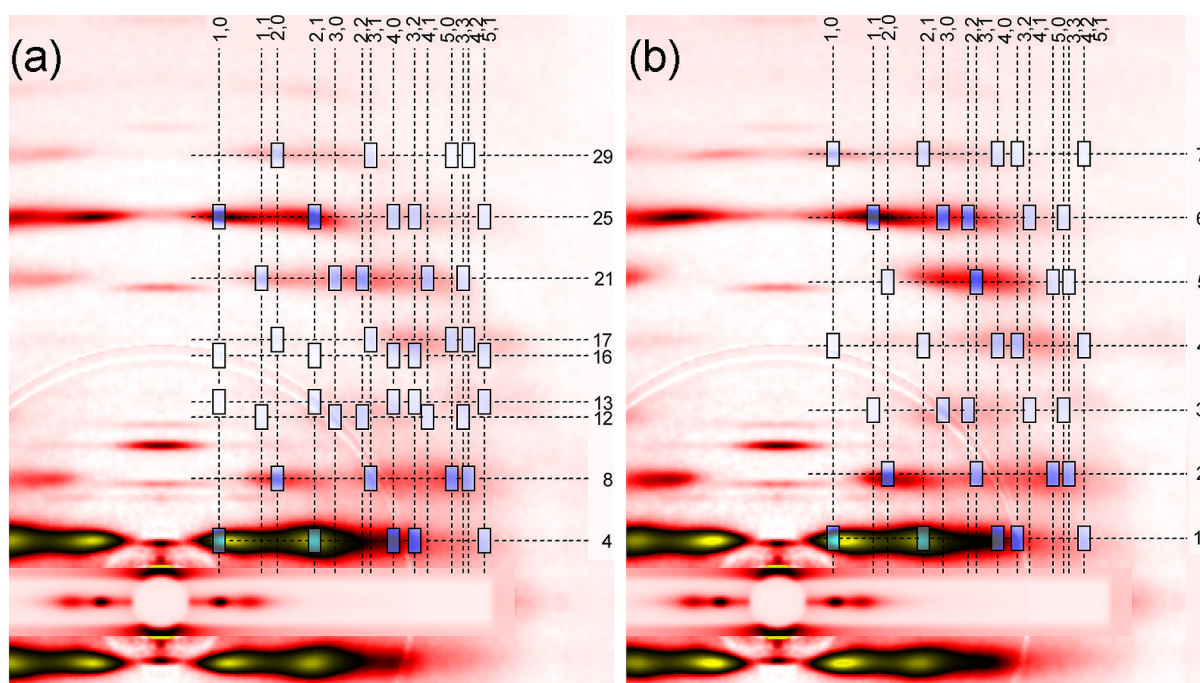
**Figure 5.**
Expected positions of crystallographic reflections due to lattice sampling. Example of human non-muscle IIA, which shows different sampling patterns depending on the absence or presence of ligand. (a), apo form; (b), ADP form. The numbers at the top of each figure represent the crystallographic indices $h$ and $k$, and those on the right represent the layer line numbers ($l$). The boxes are the positions of reflections allowed by the selection rule. The observed peaks in patterns (a) and (b) are best explained by 54/25 and 13/6 helical symmetries of actin, respectively.
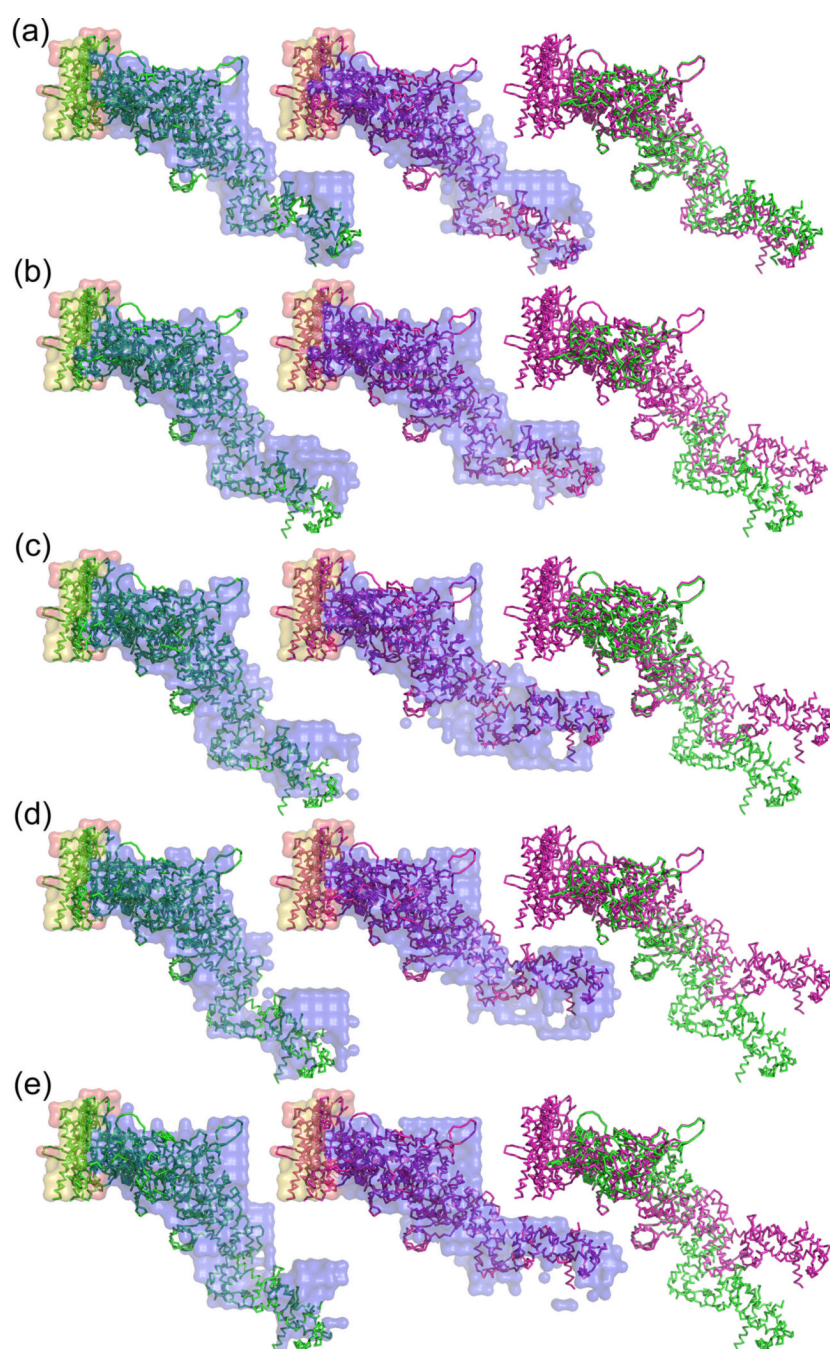
**Figure 6.**
Side-view envelope of densities of the refined acto-S1 structures (surface representation in blue, orange and pale yellow), and the best-fit α-carbon backbone structure (stick representation). (a), rabbit fast-skeletal; (b), rabbit cardiac/slow-skeletal; (c), chicken gizzard smooth; (d), human non-muscle IIA; (e), human non-muscle IIB. Left column, overlay of the density of the apo structure and the backbone; middle column, superposition of the density of the ADP structure and the backbone; right column, superposition of the apo (green) and ADP (purple) backbones. The parts of the backbones in which the apo and ADP structures perfectly coincide with each other are represented in purple (the ADP color). The blue, orange and pale yellow parts of the envelope represent S1, actin and tropomyosin, respectively. The envelope

shows the 25% level of the maximal density of the original structure. The fit between the envelope and the backbone may not seem excellent, but this is because the backbone is the one which shows the lowest discrepancy (see Figure 8), not the average. The graphics were created by PyMol.
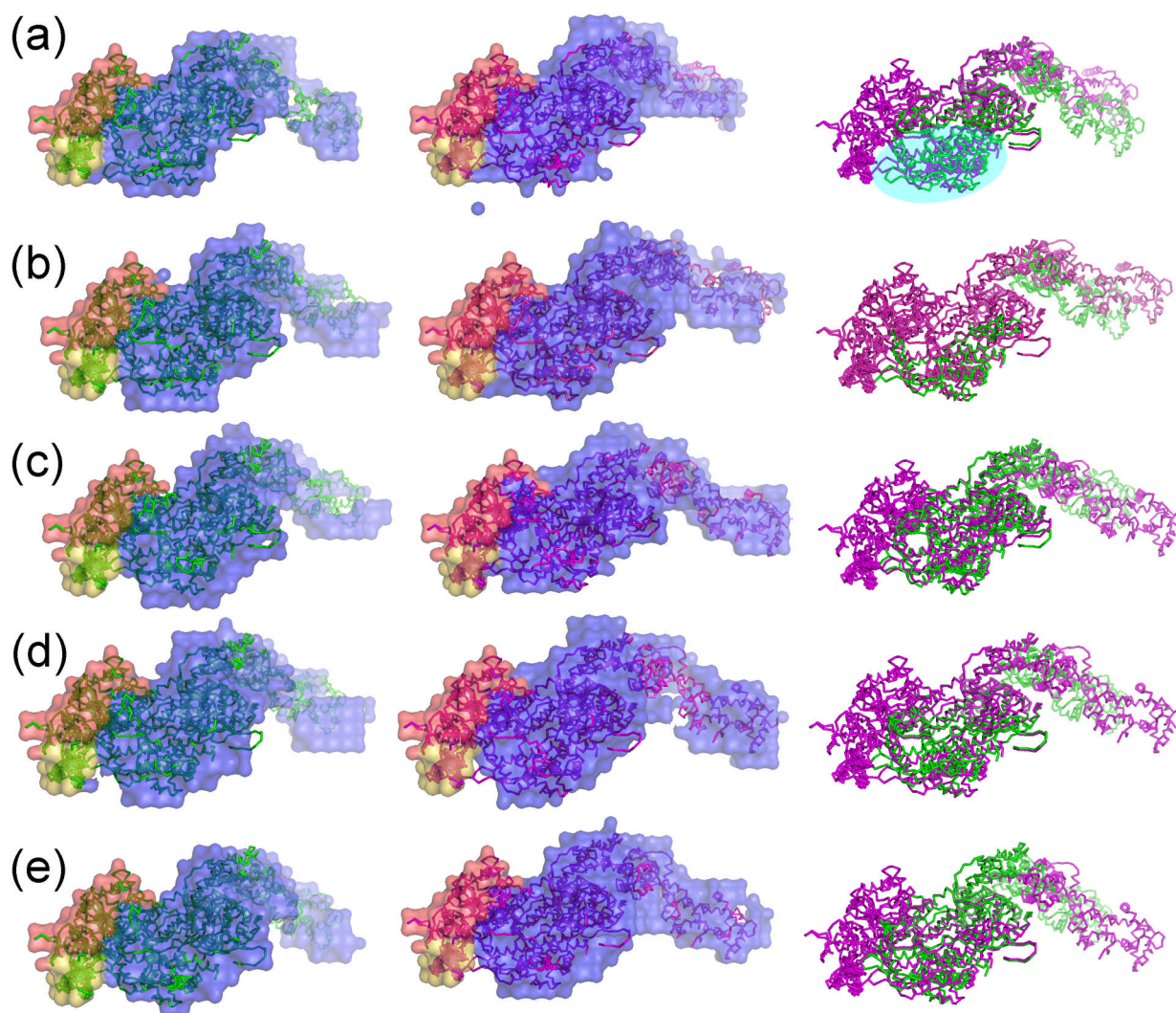
**Figure 7.**
End-on-view envelope of densities of the refined acto-S1 structures and the best-fit α-carbon backbone structure. The data are presented in the same way as in Figure 6. The upper 50K domain is marked by a sky-blue ellipse in (a).
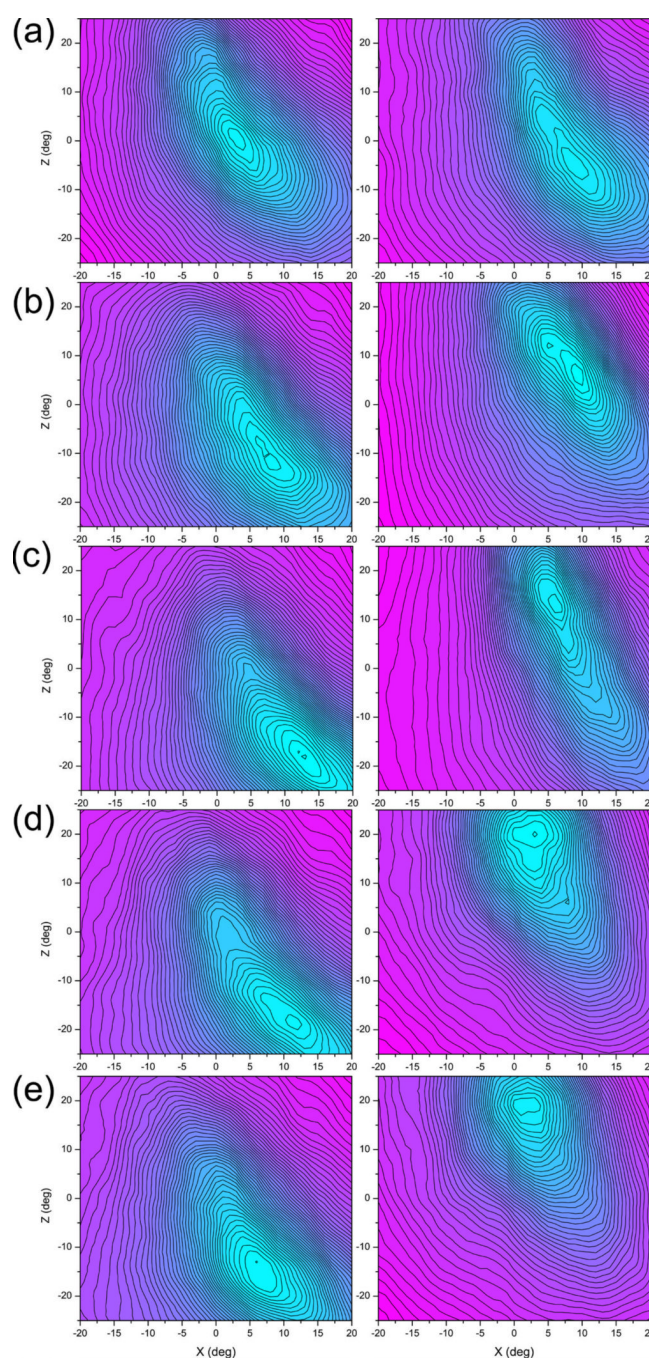
**Figure 8 .**
Discrepancy contour maps of LC-domain orientations. (a), rabbit fast-skeletal; (b), rabbit cardiac/slow-skeletal; (c), chicken gizzard smooth; (d), human non-muscle IIA; (e), human non-muscle IIB. Left column, apo structure; right column, ADP structure. The summed difference between the refined mass distribution and the mass directly calculated from the α-carbon backbone obtained from the crystal structure (see Figure 6) is presented as a function of the axial (Z) and azimuthal (X) angles of LC-domain swing, with 0° being the angle of the original Lorenz docking model for fast-skeletal S1.[24] The angles which give the lowest discrepancy (in cyan) coincide with the angles of the backbone structures shown in text-Figures 6 and 7. Although the lowest-discrepancy angles are relatively well-defined, the valley of

discrepancy tends to spread in axial direction, reflecting the spread of density of the LC domain in the refined structure (the envelopes in Figure 6).

| | skeletal | cardiac | smooth | IIA | IIB |
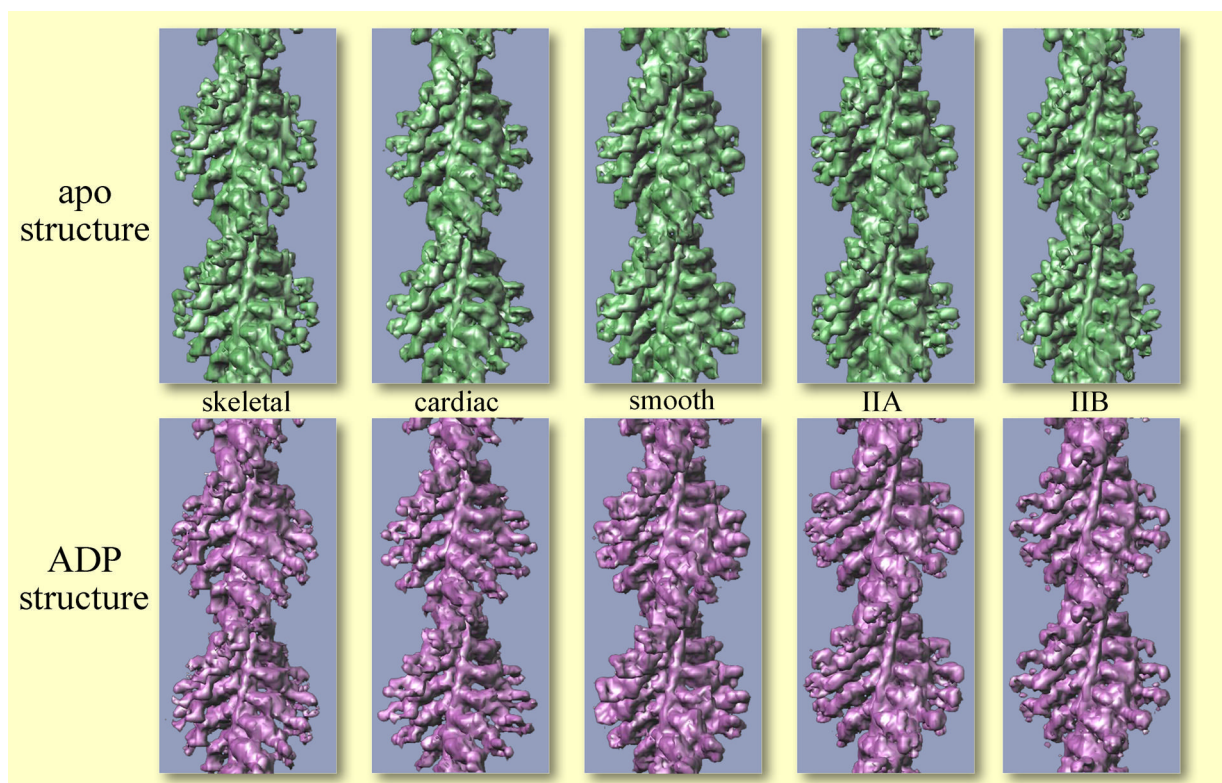
Surface-rendered 3D structures of complexes between F-actin and myosin-II subfragment-1 from various vertebrate sources, either in the presence or absence of ADP, as retrieved from X-ray fiber diffraction patterns (created by UCSF Chimera).

**Table 1**

Fitted parameters

| Source | ligand | LC (Z) | LC (X) | 50K (Z) | 50K (X) | S1 $\varphi$ | unit cell (nm) | R-factor (%) |
|--------|--------|--------|--------|---------|---------|--------------|----------------|--------------|
| Skeletal | none | 2 | 5 | 3 | −5 | −3 | 40.0 | 14.1 ± 0.2 |
|  | ADP | −5 | 17 | 0 | −14 | 0 | 40.0 | 15.1 ± 0.3 |
|  |  | $\Delta = −7$ | $\Delta = 12$ | $\Delta = −3$ | $\Delta = −9$ | $\Delta = 3$ |  |  |
| Cardiac | none | −12 | 16 | 3 | −13 | −1 | 39.0 | 13.9 ± 0.2 |
|  | ADP | 6 | 19 | 1 | −19 | −1 | 39.2 | 13.2 ± 0.2 |
|  |  | $\Delta = 18$ | $\Delta = 3$ | $\Delta = −2$ | $\Delta = −6$ | $\Delta = 0$ |  |  |
| Gizzard | none | −16 | 24 | 4 | −16 | −5 | 41.2 | 13.1 ± 0.3 |
|  | ADP | 13 | 13 | 6 | −11 | −12 | 41.2 | 13.2 ± 0.2 |
|  |  | $\Delta = 29$ | $\Delta = −11$ | $\Delta = 2$ | $\Delta = 5$ | $\Delta = −7$ |  |  |
| IIA | none | −16 | 18 | 2 | −18 | −2 | 39.8 | 14.8 ± 0.3 |
|  | ADP | 20 | 6 | 3 | −9 | −1 | 42.2 | 13.6 ± 0.4 |
|  |  | $\Delta = 36$ | $\Delta = −12$ | $\Delta = 1$ | $\Delta = 9$ | $\Delta = 1$ |  |  |
| IIB | none | −16 | 13 | −3 | −24 | 1 | 39.6 | 14.2 ± 0.2 |
|  | ADP | 19 | 1 | 2 | −13 | 0 | 41.9 | 13.3 ± 0.3 |
|  |  | $\Delta = 35$ | $\Delta = −12$ | $\Delta = 5$ | $\Delta = 11$ | $\Delta = −1$ |  |  |

LC and 50K refer to angles of swing of the light chain domain and the upper 50K domain, respectively. Z and X refer to the axial and azimuthal directions. S1 $\varphi$ refers to the angle of rotation of the whole S1 molecule around its long axis. The angles are relative to the values for the original Lorenz docking model for fast-skeletal S1. Unit cell size refers to that of the superlattice formed by the thin filaments of skeletal muscle fibers (see text for details), and the values were determined in the course of iterative refinement process. The R-factor is expressed as the mean from six independent runs ± standard deviation (%), where R-factor = $(\sum ||F_{obs}| − |F_{calc}||) / \sum |F_{obs}|$, and $F_{obs}$ and $F_{calc}$ are the observed and calculated structure factors, respectively.

**Table 2**

Additional fitted parameters not listed in Table 1.

| Source | ligand | RLC | ELC | TM | Cont(1) | Cont(2) | Cont(3) | Cont(4) | Cont(5) | Cont(6) | Cont(7) |
|---|---|---|---|---|---|---|---|---|---|---|---|
| Skeletal | rigor | 0.55 | 0.99 | 0.6 | 0.49 | 0.68 | 0.59 | 0.82 | 0.74 | 0.5 | 0.6 |
| | ADP | 0.5 | 0.99 | 0.56 | 0.63 | 0.87 | 0.78 | 0.74 | 0.72 | 0.58 | 0.84 |
| Cardiac | rigor | 0.5 | 0.99 | 0.6 | 0.44 | 0.66 | 0.53 | 0.55 | 0.66 | 0.63 | 0.85 |
| | ADP | 0.88 | 0.88 | 0.6 | 0.48 | 0.89 | 0.61 | 0.58 | 0.93 | 0.69 | 0.67 |
| Gizzard | rigor | 0.73 | 1 | 0.58 | 0.44 | 0.72 | 0.5 | 0.99 | 0.77 | 0.56 | 0.74 |
| | ADP | 0.84 | 0.71 | 0.48 | 0.59 | 0.92 | 1 | 1 | 1 | 1 | 0.72 |
| IIA | rigor | 0.66 | 0.99 | 0.6 | 0.29 | 0.67 | 0.69 | 0.75 | 0.78 | 0.61 | 0.7 |
| | ADP | 0.85 | 0.9 | 0.6 | 0.34 | 0.74 | 1 | 1 | 1 | 0.73 | 0.81 |
| IIB | rigor | 0.74 | 1 | 0.58 | 0.24 | 0.51 | 0.76 | 0.58 | 0.93 | 0.96 | 0.77 |
| | ADP | 0.99 | 0.96 | 0.6 | 0.27 | 0.58 | 1 | 1 | 1 | 0.66 | 0.5 |

Parameters fitted in the third step and not listed in Table 1 are listed here. Cont refers to the fitted fraction of the continuous component of ALL versus sampled component. The number in the parentheses refers to the layer line number (based on 13/6 symmetry of actin).

**Table 3**

Parameters before refinement

| Source | ligand | LC(Z) | LC(X) | 50K(Z) | 50K(X) | S1 φ | RLC | ELC | TM | Symmetry |
|--------|--------|-------|-------|--------|--------|------|-----|-----|------|----------|
| Skeletal | rigor | 2 | 4 | 0 | −6 | −3 | 0.46 | 0.7 | 0.6 | 54/25 |
| | ADP | 2 | 12 | −4 | −14 | 0 | 0.5 | 0.7 | 0.56 | 54/25 |
| Cardiac | rigor | −2 | 8 | 4 | −12 | −1 | 0.68 | 0.78 | 0.6 | 54/25 |
| | ADP | 4 | 16 | 4 | −8 | −1 | 0.74 | 0.86 | 0.6 | 54/25 |
| Gizzard | rigor | −6 | 14 | 4 | −12 | −5 | 0.74 | 0.84 | 0.58 | 54/25 |
| | ADP | 6 | 14 | 2 | −16 | −11 | 0.56 | 0.66 | 0.48 | 54/25 |
| IIA | rigor | −6 | 8 | 0 | −14 | −2 | 0.7 | 0.8 | 0.6 | 54/25 |
| | ADP | 12 | 4 | 4 | −2 | −1 | 0.78 | 0.88 | 0.6 | 13/6 |
| IIB | rigor | −6 | 6 | −6 | −24 | 1 | 0.72 | 0.82 | 0.58 | 54/25 |
| | ADP | 12 | 4 | 2 | −8 | −1 | 0.8 | 0.88 | 0.6 | 13/6 |

The values obtained in the first step (before refinement) are listed here. RLC, ELC, and TM refer to the relative occupancy of regulatory and essential light chains and tropomyosin chain, respectively. Symmetry refers to that of F-actin that best explains the lattice sampling pattern of ALL's (determined by visual inspection of the diffraction pattern).

**Table 4**

cross-correlated normalized spatial discrepancy (NSD)[50]

| source and ligand | NSD ± SD (n = 15) |
| --- | --- |
| Skeletal-rigor | $0.463 \pm 0.051$ |
| Skeletal-ADP | $0.440 \pm 0.027$ |
| Cardiac-rigor | $0.539 \pm 0.044$ |
| Cardiac-ADP | $0.445 \pm 0.046$ |
| Gizzard-rigor | $0.421 \pm 0.015$ |
| Gizzard-ADP | $0.507 \pm 0.077$ |
| IIA-rigor | $0.448 \pm 0.024$ |
| IIA-ADP | $0.398 \pm 0.006$ |
| IIB-rigor | $0.478 \pm 0.071$ |
| IIB-ADP | $0.421 \pm 0.044$ |

SD is the standard deviation.